

# **Generation of highly-retrievable atom–photon entanglement with a millisecond lifetime via a spatially-multiplexed cavity**

Minjie Wang, Shengzhi Wang, Tengfei Ma, Ya Li, Yan Xie, Haole Jiao,  
Hailong Liu, Shujing Li, Hai Wang<sup>\*</sup>

The State Key Laboratory of Quantum Optics and Quantum Optics  
Devices, Institute of Opto-Electronics, Shanxi University, Taiyuan

030006

China Collaborative Innovation Center of Extreme Optics,  
Shanxi University, Taiyuan 030006, China

Qubit memory that is entangled with photonic qubit is the building block for long-distance quantum repeaters. Cavity-enhanced and long-lived spin-wave–photon entanglement has been demonstrated by applying dual laser beams onto optical-lattice atoms. However, owing to cross readouts by two beams, retrieval efficiency of spin-wave qubit is decreased by one quarter compared to that of single-mode spin wave at all storage times. Here, by coupling cold atoms to two modes of a polarization-interferometer-based cavity, we achieve perfect qubit retrieval in cavity-enhanced and long-lived atom-photon entanglement. A write-laser beam is applied onto cold atoms, we then create a magnetic-field-insensitive spin-wave qubit that is entangled with the

photonic qubit encoded onto two arms of the interferometer. The spin-wave qubit is retrieved by a read beam, which avoids the cross readouts. Our experiment demonstrates  $540\mu\text{s}$  storage time at 50% intrinsic qubit retrieval efficiency, which is 13.5 times longer than the best reported result.

**Introduction.** — An qubit memory entangled with a photonic qubit forms the building block (repeater node) for long-distance quantum communications [1-3], large-scale quantum interworks [4-5], and quantum clock network [6] through a quantum repeater (QR) [1-2]. It also may be used for scalable linear-optical quantum computations [7]. In past decades, optical quantum memories (QMs) have been experimentally demonstrated with various matter systems [8] such as atomic ensembles [1, 9] and single-quantum systems including individual atoms [10-11], ions [12], and solid-state spins [13-14]. Compared with the QMs in a single-quantum system, the atomic-ensemble-based QMs feature collective enhancement and promise higher retrieval efficiencies [1]. For example, the highest retrieval efficiency for a single-photon qubit stored in a single atom trapped in a high-finesse optical cavity is 22% [11], while that in a high-optical-depth cold atomic ensemble is 85% [15]. With atomic ensembles, optical QMs has been demonstrated via various schemes [8-9, 16-17] including Duan–Lukin–Cirac–Zoller (DLCZ) protocol [1, 18-40] and “read-write” [16] (or called “absorptive” [17]) schemes such as electromagnetically-induced-transparency (EIT) dynamics [15, 41-51], photon echoes [52-59], Raman memory [60-62] and its variants [63-64], etc. In contrast to the “read-write” schemes, the DLCZ protocol establishes QMs via spontaneous Raman emissions of Stokes photon induced by a write pulse instead of storing single specific

(incoming) photons [16]. Since DLCZ protocol can directly produces non-classically correlated [18-30] or entangled [31-40] pairs of a Stokes photon and a spin-wave memory, it benefits for practically realizing QRs.

High-efficiency and long-lived QMs are required for effectively achieving quantum information tasks [3, 7]. In long-distance entanglement distribution through QRs, a 1% increase in retrieval efficiency can improve the repeater rate by 10–14% [1]. The lifetime at 50% efficiency is defined as a benchmark of memory nodes in QRs [3]. Additionally, establishing entanglement between two nodes separated by  $L=300$  km in a “heralded” fashion requires storing a qubit for at least  $L/c=1.5$  ms [36, 65], with  $c$  being the speed of light in fibers. To realize long-lived QMs, significant progresses have been made with cold atomic ensembles [21-26, 34-36, 56]. These studies show that atomic-motion-induced decoherence can be suppressed either by lengthening spin-wave wavelengths [22-23, 34, 36, 56] or confining the atoms in optical lattices [24-26, 34-35]. Inhomogeneous-broadening-induced decoherence may be suppressed by storing SWs in magnetic-field-insensitive (MFI) coherences, which includes three spin transitions  $|5S_{1/2}, F=1, m_F=\pm 1, 0\rangle \leftrightarrow |5S_{1/2}, F=2, m_F=\mp 1, 0\rangle$  for  $^{87}\text{Rb}$  atoms, where,  $m_{F_1}=0 \leftrightarrow m_{F_2}=0$  is called clock coherence.

In previous long-lived atom–photon entanglement generation via DLCZ protocol [34], a Mach–Zehnder interferometer, whose two arms

are used to encode photonic qubit, is built around optical-lattice Rb atoms. Two spatially-distinctive SWs associated with the clock coherence and correlated with the Stokes emissions into the two arms, are created by a write beam and stored as memory qubit. To maintain maximal entanglement, the relative phase between the two arms was actively stabilized. The lifetime of entanglement storage reaches 0.1 s but the retrieval efficiency is only  $\sim$ 16% due to weak atom-photon interactions [34]. The high-efficiency qubit memories have been achieved by using either high-optical-depth cold atoms [15, 50] or moderate-optical-depth atoms coupled with a low-finesse optical cavity [23, 26, 32, 35]. Using the cavity-coupling scheme, Pan's group demonstrated intrinsic retrieval efficiency up to  $\sim$ 76% in a DLCZ experiment that create polarization atom-photon entanglement [32]. In that experiment, the spin-wave qubit is stored as superimposition of magnetic-field-sensitive and MFI coherences. Limiting to fast decoherence of the magnetic-field-sensitive coherence, the memory lifetime is only  $\sim$ 30  $\mu$ s [32]. Efficient and long-lived atom-photon quantum correlations has been demonstrated by applying a write beam onto optical-lattice atoms, where the atomic SW is stored in the clock coherence and coupled to a ring cavity [26]. The zero-delay efficiency reaches to 76% and at 50-ms storage time to 50%. Next, Pan's group demonstrated cavity-enhanced atom-photon entanglement with sub-second lifetime [35]. To create H- and V-

polarized Stokes emissions of photonic qubit, the group applied two write beams onto the lattice atoms. The two SW modes, both associated with the clock coherence and correlated with the H- and V- polarized Stokes fields, respectively, are stored as memory qubit. That experiment [35] removes the M-Z interferometer used in Ref. [34] and then avoids experimental complexity due to interferometer-mediated coupling between atoms and a cavity. However, that experiment requires dual read-laser beams to retrieve the two SWs, which leads to cross retrievals and decrease qubit retrieval efficiency by one quarter compared to that of a single-mode SW at all storage times. For example, the efficiency of retrieving the qubit was  $\sim 58\%$  at zero delay [35], about three quarters that of the single-mode one ( $\sim 76\%$ ) [26]. So far, perfect-cavity-enhanced qubit retrievals in long-lived atom-photon entanglement remain a challenge. Here, we overcome this challenge by coupling cold atoms to a two-mode ring cavity based on a polarization interferometer. The interferometer is mainly formed by two beam displacers (BD1 and BD2) and then phase-passively stabilized. Two optical lenses are inserted in the interferometer, which make interferometer's two arms ( $A_R$  and  $A_L$ ) crossway pass-through cold atoms. By arranging interferometer's configuration, the ring cavity simultaneously supports the two arms as cavity modes. By applying a write beam, we create two SWs associated with the clock coherence and correlated with the Stokes emissions into

the cavity modes  $A_R$  and  $A_L$ , respectively. The two SWs are retrieved by a read beam, which avoids the cross retrieval. The two Stokes (anti-Stokes) fields forms a photonic qubit and resonate with the cavity. The intrinsic qubit retrieval efficiencies reach 50% (66.7%) at 540- $\mu$ s (230- $\mu$ s) storage time, which is 13.5 (24) times longer than the best reported results [35] ([32]). The measured Bell parameter for atom-photon entanglement is  $2.5 \pm 0.02$  at zero delay. Unlike previous experiments with SWs being directly coupled into a cavity [23, 32, 35, 66-67], our experiment demonstrated interferometer-mediated coupling between SWs and a cavity, which enable a perfect retrieval in cavity-enhanced and long-lived atom-photon entanglement.

As shown in the schematic diagram Fig.1a, the heart of experimental setup is a ring cavity inserted by a polarization interferometer (circled by dashed line). The ring cavity is formed by three flat mirrors ( $HR_{1,2,3}$ ) with high reflection and a flat output coupler (OC) with a reflectance of 80%. It supports  $TEM_{00}$  mode  $A_{00}$  that propagates in the whole cavity [68]. When the polarization interferometer is inserted in the cavity, the  $A_{00}$  mode only propagates in the path from BD2 to BD1 via OC and  $HR_1$  (black line in Fig.1a). When  $A_{00}$  propagates along clockwise, it is split into  $H$  (horizontally) and  $V$  (vertically) -polarized components by BD2, both direct into the interferometer's arms  $A_L$  and  $A_R$ , respectively. Two identical optical lenses lens1 and lens2 with a focus length  $F_0$ , are

inserted in the interferometer. Then, the arms  $A_L$  and  $A_R$  crossway pass through the atoms and couple with the atoms, respectively. The more detailed explanations of the  $A_L$  and  $A_R$  paths can be found in Supplementary material [68]. By setting the distance between lens1 and lens2 to be  $2F_0$ , the two arms are well recombined into the mode  $A_{00}$  by BD1 and then supported by the cavity. In our experiment, the spot size of  $A_{00}$  is set to be a large value (5.2mm) in order to decrease the mode losses escaping from the cavity. The measured loss of the mode  $A_{00}$  via  $A_R$  ( $A_L$ ) path escaping from cavity per round trip is  $\sim 3.2\%$  (3.2%). So, the  $A_R$  and  $A_L$  arms may serve as cavity modes.

The atomic ground levels  $|a\rangle = |5S_{1/2}, F=1\rangle$  and  $|b\rangle = |5S_{1/2}, F=2\rangle$  together with the excited level  $|e_1\rangle = |5P_{1/2}, F'=1\rangle$  ( $|e_2\rangle = |5P_{1/2}, F'=2\rangle$ ) form a  $\Lambda$ -type system [Fig.1b and c]. After the atoms are prepared in the Zeeman state  $|a, m_{F_a} = 0\rangle$ , we start spin-wave-photon (atom-photon) entanglement generation. At the beginning of a trial [68], a 795-nm  $\sigma^+$ -polarized write pulse with red-detuned by 110 MHz to the  $|a\rangle \rightarrow |e_1\rangle$  transition is applied to the atoms along  $z$ -axis through a beam splitter BS1. This write pulse induces the Raman transition  $|a, m_{F_a} = 0\rangle \rightarrow |b, m_{F_b} = 0\rangle$  via  $|e_1, m_{F_e} = 1\rangle$  [Fig. 1b], which emit  $\sigma^+$ -polarized Stokes photons and simultaneously create SW excitations associated with the clock coherence  $|m_a = 0\rangle \leftrightarrow |m_b = 0\rangle$ . If the Stokes photon is emitted into the cavity mode  $A_R$  ( $A_L$ ) and moves towards the right, one excitation will be created in the SW mode  $M_R$  ( $M_L$ ) defined by the wave-vector  $k_{M_R} = k_w - k_{S_R}$  ( $k_{M_L} = k_w - k_{S_L}$ ), where  $k_w$  is the wave-vector of the write pulse and  $k_{S_R}$  ( $k_{S_L}$ ) that of the Stokes photon in the cavity  $A_R$  ( $A_L$ ) mode. The angle between the mode  $A_R$  ( $A_L$ ) and the

write beam is  $\theta_R \approx 0.053^\circ$  ( $\theta_A \approx -0.053^\circ$ ) [68]. Such small angles make SW wavelengths be long, suppressing atomic-motion-induced decoherence [36]. The  $\sigma^+$ -polarized Stokes fields in  $A_R$  and  $A_L$  modes propagate along clockwise, which are transformed into  $H$ -polarized fields by a  $\lambda/4$  wave-plate QWs. Furthermore, the  $H$ -polarized field in  $A_L$  is transformed into  $V$ -polarized field by a  $\lambda/2$  wave-plate HWs. Both fields are combined into the cavity mode  $A_{00}$  by BD2 and form a Stokes qubit  $S_{qbit}$ . As shown in Fig. 1(b), the write pulse also induces the Raman transition  $|a, m_{Fa} = 0\rangle \rightarrow |b, m_{Fb} = 2\rangle$  via  $|e_1, m_{Fe} = 1\rangle$ , which emit  $\sigma^-$ -polarized Stokes photons and simultaneously create SWs associated with the magnetic-field-sensitive coherence  $|m_{Fa} = 0\rangle \leftrightarrow |m_{Fb} = 2\rangle$ . If the  $\sigma^-$ -polarized Stokes photon direct into the mode  $A_R$  ( $A_L$ ) and propagate along clockwise, it will be transformed into  $V$ - ( $H$ -) polarized photon by the QWs (QWs and HWs) and then is excluded from the  $A_{00}$  cavity mode by BD2. Propagating in  $A_{00}$ , the  $S_{qbit}$  returns the interferometer. It is split into  $H$  and  $V$ -polarized fields by BD1, which direct into  $A_R$  and  $A_L$  modes, respectively. Both Stokes modes are transformed into  $\sigma^+$ -polarization by wave-plates and then interact with the atoms again. The spin-wave qubit formed by  $M_R$  and  $M_L$  modes is entangled with  $S_{qbit}$ , which is written as:

$$\Phi_{ap} = (|H\rangle_S |M_R\rangle + e^{i\varphi_s} |V\rangle_S |M_L\rangle) / \sqrt{2} \quad (1)$$

where,  $|H\rangle_S$  ( $|V\rangle_S$ ) denotes the  $H$ - ( $V$ -) polarized Stokes photon,  $|M_R\rangle$  ( $|M_L\rangle$ ) one SW excitation in the mode  $M_R$  ( $M_L$ ),  $\varphi_s$  the relative phase between the two Stokes emissions from the atoms to BD2 via  $A_R$  and  $A_L$  paths.

After a storage time  $t$ , we apply a  $\sigma^+$ -polarized read pulse onto the atoms through a beam splitter BS2. The read pulse is red-detuned by 110

MHz to the  $|b\rangle \rightarrow |e_2\rangle$  transition and counter-propagates with the write beam, which convert the spin-wave  $|M_R\rangle$  ( $|M_L\rangle$ ) into an anti-Stokes photon. The anti-Stokes photon retrieved from  $|M_R\rangle$  ( $|M_L\rangle$ ) is  $\sigma^+$ -polarized and emitted into the mode determined by the wave-vector constraint  $k_{AS_R} \approx -k_{S_R}$  ( $k_{AS_L} \approx -k_{S_L}$ ), it propagates along anti-clockwise in the arm  $A_R$  ( $A_L$ ). The anti-Stokes fields in  $A_R$  and  $A_L$  are transformed into  $H$ -polarized fields by a  $\lambda/4$ -plate  $QW_{AS}$ . Furthermore, the anti-Stokes field in  $A_L$  is transformed into  $V$ -polarized field by a  $\lambda/2$ -plate  $HW_{AS}$ . Both fields are combined into an anti-Stokes qubit  $AS_{qbit}$  by BD1 and then propagate in  $A_{00}$  mode. The  $AS_{qbit}$  is split into  $H$ - and  $V$ -polarized fields by BD2, which direct into  $A_R$  and  $A_L$  modes, respectively. Next, both anti-Stokes modes are transformed into  $\sigma^+$ -polarization by wave-plates and then interact with the atoms. So, the atoms are repeatedly coupled with the cavity modes. The two-photon entangled state is written as:

$$\Phi_{p-p} = \left( |H\rangle_S |H\rangle_{AS} + e^{i(\varphi_S + \varphi_{AS})} |V\rangle_S |V\rangle_{AS} \right) / \sqrt{2} \quad (2).$$

where, the subscript  $S$  ( $AS$ ) denotes the Stokes (anti-Stokes) photon,  $\varphi_{AS}$  the relative phase between the two anti-Stokes emissions from the atoms to BD1 via  $A_R$  and  $A_L$  paths. In our experiment, the sum of  $\varphi_S$  and  $\varphi_{AS}$  is passively set to zero with a phase compensator [68]. The cavity length is actively stabilized by coupling a cavity-locking beam through OC. The Stokes and anti-Stokes fields are tuned to resonate with the ring cavity [68]. As shown in Fig.1, the escaped Stokes (anti-Stokes) photon from OC is coupled to a sing-mode fiber and guided into a polarization-beam splitter  $PBS_S$  ( $PBS_{AS}$ ). Two outputs of  $PBS_S$  ( $PBS_{AS}$ ) are sent to

single-photon detectors  $D_1$  ( $D_3$ ) and  $D_2$  ( $D_4$ ). The polarization angle  $\theta_s$  ( $\theta_{AS}$ ) of the Stokes (anti-Stokes) field is changed by rotating a  $\lambda/2$ -plate before PBS<sub>S</sub> (PBS<sub>AS</sub>).

The intrinsic retrieval efficiency of the SW qubit can be measured as

$R_{qbit}^{inc} = P_{S, AS} / (\eta_{TD} P_S)$ , where  $P_{S, AS} = P_{D_1, D_3} + P_{D_2, D_4}$ ;  $P_{D_1, D_3}$  ( $P_{D_2, D_4}$ ) is the probability of detecting a coincidence between the detectors  $D_1$  ( $D_2$ ) and  $D_3$  ( $D_4$ ) for  $\theta_s = \theta_{AS} = 0^\circ$ ,  $P_S = P_{D_1} + P_{D_2}$ , where  $P_{D_1}$  ( $P_{D_2}$ ) is the probability of detecting a Stokes photon at  $D_1$  ( $D_2$ );  $\eta_{TD} \approx 15\%$  is the total detection efficiency of the anti-Stokes channel [68]. Moreover, the intrinsic retrieval efficiency for an individual SW  $M_L$  ( $M_R$ ) mode is defined as  $R_L^{inc} = P_{D_1, D_3} / (\eta_{TD} P_{D_1})$  ( $R_R^{inc} = P_{D_2, D_4} / (\eta_{TD} P_{D_2})$ ). Fig.2 plots the measured efficiencies  $R_{qbit}^{inc}$  (red circle dots),  $R_L^{inc}$  (blue square dots), and  $R_R^{inc}$  (green triangle dots) as functions of storage time  $t$ . From the figure, we see that  $R_{qbit}^{inc} \approx R_L^{inc} \approx R_R^{inc}$  for different times  $t$ , which means that the retrieval efficiency for an SW qubit is the same as that for a single-mode SW. This shows that the efficiency loss of retrieving the qubit, which is a key limit in state-of-the-art work [35], is overcome in our experiment. The solid grey curve is the fit to the retrieval efficiencies  $R_{qbit}^{inc}$ ,  $R_L^{inc}$ , and  $R_R^{inc}$  according to the function  $R(t) = R_0 (\exp(-t^2/\tau_0^2) + \exp(-t/\tau_0)) / 2$ , which yields retrieval efficiencies  $R_0 = 77\%$ ,  $R(t = 0.23\text{ms}) \approx 66.7\%$  and  $R(t = 0.54\text{ms}) \approx 50\%$ , together with a memory lifetime  $\tau_0 \approx 1\text{ms}$ .

Next, we measure the Bell-type Clauser–Horne–Shimony–Holt (CHSH)

inequality to confirm the spin-wave-photon entanglement state  $\Phi_{a-p}$ . The Bell CHSH parameter is defined as

$$S_{Bell} = |E(\theta_S, \theta_{AS}) - E(\theta_S, \theta'_{AS}) + E(\theta'_S, \theta_{AS}) + E(\theta'_S, \theta'_{AS})| < 2 \quad \text{with the correlation function } E(\theta_S, \theta_{AS}), \quad \text{which is written as}$$

$$\frac{C_{13}(\theta_S, \theta_{AS}) + C_{24}(\theta_S, \theta_{AS}) - C_{14}(\theta_S, \theta_{AS}) - C_{23}(\theta_S, \theta_{AS})}{C_{13}(\theta_S, \theta_{AS}) + C_{24}(\theta_S, \theta_{AS}) + C_{14}(\theta_S, \theta_{AS}) + C_{23}(\theta_S, \theta_{AS})}.$$

For example,  $C_{13}(\theta_S, \theta_{AS})$  ( $C_{24}(\theta_S, \theta_{AS})$ ) denotes the coincidence counts between the detectors  $D_1$  ( $D_2$ ) and  $D_3$  ( $D_4$ ) for the polarization angles  $\theta_S$  and  $\theta_{AS}$ . We used the canonical settings  $\{\theta_S=0^\circ, \theta'_S=45^\circ, \theta_{AS}=22.5^\circ, \text{ and } \theta'_{AS}=67.5^\circ\}$  in measuring the  $S_{Bell}$ . Fig. 3 shows the decay of  $S_{Bell}$  as a function of storage time  $t$  for  $\chi=2\%$ . At  $t \approx 0 \mu\text{s}$ ,  $S_{Bell} = 2.5 \pm 0.02$ , while at  $t = 1.15 \text{ ms}$ ,  $S_{Bell} = 2.05 \pm 0.03$ . These violate the Bell inequality by 25 and 1.7 standard deviations, respectively.

For comparison, we plot Fig. S4 in Supplementary material [68] to show the measured retrieval efficiencies for the qubit storages as functions of storage times in previous works [11, 15, 32, 34, 35, 45, 50]. Our result of storage time of 540  $\mu\text{s}$  (230  $\mu\text{s}$ ) at 50% (66.7%) retrieval efficiency is 13.5 (24) times longer than the previously reported best result [35] ([32]).

**Conclusion.** —The use of the polarization interferometer in the cavity enables us to apply a write beam to create two SW modes of the memory qubit, both associated with the clock coherence and coupled to the ring cavity. Thanks to phase-matching condition, the two SW modes are retrieved by a read beam, which avoids the cross retrievals in Ref. [35].

The relative phase between the two arms is passively stabilized and easily set to be zero with the phase compensator. On this basis, we achieve quadruple resonance of the cavity with the Stokes and retrieved fields propagating in the cavity modes  $A_R$  and  $A_L$ , respectively. This represents the first demonstration of an atomic ensemble simultaneously coupled into two  $\text{TEM}_{00}$  modes of a cavity. We achieve atom-photon entanglement with highly-retrievable efficiency (77%) and millisecond lifetime. By selecting more cavity modes to couple with the atoms, we will achieve massively-multiplexed and high-reversible spin-wave-photon entanglement with long lifetime and then is used for achieving long-distance (1000-km) entanglement distributions through QR [68].

We suppress inhomogeneous-broadening-induced decoherence by storing both SWs in the clock coherence. Atomic-motion-induced dephasing is suppressed by using the storage scheme of the long-wavelength SW [36]. The lifetime in our presented experiment is  $\sim 1$  ms, which can be extended to hundreds of milliseconds by loading the cold atoms into optical lattices and using magic field values [35].

## Acknowledgment

We acknowledge funding support from Key Project of the Ministry of Science and Technology of China (Grant No. 2016YFA0301402); The National Natural Science Foundation of China (Grants: No. 11475109, No. 11974228), Fund for Shanxi “1331 Project” Key Subjects Construction.

\*Corresponding author: wanghai@sxu.edu.cn

## References:

- [1] N. Sangouard, C. Simon, H. de Riedmatten, and N. Gisin, *Rev. Mod. Phys.* **83**, 33 (2011).
- [2] L. M. Duan, M. D. Lukin, J. I. Cirac, and a. P. Zoller, *Nature* **414**, 413 (2001).
- [3] C. Simon, *Nat. Photon.* **11**, 678 (2017).
- [4] H. J. Kimble, *Nature* **453**, 1023 (2008).
- [5] S. Wehner, D. Elkouss, and R. Hanson, *Science* **362**, 303 (2018).
- [6] P. Kómár, E. M. Kessler, M. Bishof, L. Jiang, A. S. Sørensen, J. Ye, and M. D. Lukin, *Nat. Phys.* **10**, 582 (2014)
- [7] S. D. Barrett, P. P. Rohde, and T. M. Stace, *New J. Phys.* **12**, 093032 (2010).
- [8] F. Bussières, N. Sangouard, M. Afzelius, H. de Riedmatten, C. Simon,

and W. Tittel, *Journal of Modern Optics* **60**, 1519 (2013).

[9] A. I. Lvovsky, B. C. Sanders, and W. Tittel, *Nat. Photon.* **3**, 706 (2009).

[10] T. van Leent, M. Bock, R. Garthoff, K. Redeker, W. Zhang, T. Bauer, W. Rosenfeld, C. Becher, and H. Weinfurter, *Phys. Rev. Lett.* **124**, 010510 (2020).

[11] M. Körber, O. Morin, S. Langenfeld, A. Neuzner, S. Ritter, and G. Rempe, *Nat. Photon.* **12**, 18 (2017).

[12] B.B. Blinov, D.L. Moehring, L.-M Duan, C. Monroe, *Nature* **428**, 153 (2004).

[13] B. Hensen, H. Bernien, A. E. Dreau, A. Reiserer, N. Kalb, M. S. Blok, J. Ruitenberg, R. F. Vermeulen, R. N. Schouten, C. Abellan, W. Amaya, V. Pruneri, M. W. Mitchell, M. Markham, D. J. Twitchen, D. Elkouss, S. Wehner, T. H. Taminiau, and R. Hanson, *Nature* **526**, 682 (2015).

[14] A. Delteil, Z. Sun, W.-b. Gao, E. Togan, S. Faelt, and A. Imamoğlu, *Nat. Phys.* **12**, 218 (2015).

[15] Y. Wang, J. Li, S. Zhang, K. Su, Y. Zhou, K. Liao, S. Du, H. Yan, and S.-L. Zhu, *Nat. Photon.* **13**, 346 (2019).

[16] Mikael Afzelius, Nicolas Gisin, and Hugues de Riedmatten, *Quantum memory for photons*, *Physics Today* **68**, 12, 42 (2015).

[17] K. Heshami, D. G. England, P. C. Humphreys, P. J. Bustard, V. M.

Acosta, J. Nunn, and B. J. Sussman, *Journal of Modern Optics* **63**, 2005 (2016).

- [18] A. Kuzmich, W. P. Bowen, A. D. Boozer, A. Boca, C. W. Chou, L.-M. Duan, and a. H. J. Kimble, *Nature* **423**, 731 ( 2003).
- [19] Julien Laurat, Hugues de Riedmatten, Daniel Felinto, Chin-Wen Chou, E. W., Schomburg, and a. H. J. Kimble., *Opt. Express* **14**, 6912 (2006).
- [20] J. Simon, H. Tanji, J. K. Thompson, and V. Vuletic, *Phys. Rev. Lett.* **98**, 183601 (2007).
- [21] D. Felinto, C. W. Chou, H. de Riedmatten, S. V. Polyakov, and H. J. Kimble, *Phys. Rev. A* **72**, 053809 (2005).
- [22] B. Zhao, Y.-A. Chen, X.-H. Bao, T. Strassel, C.-S. Chuu, X.-M. Jin, J. Schmiedmayer, Z.-S. Yuan, S. Chen, and J.-W. Pan, *Nat. Phys.* **5**, 95 (2008).
- [23] X.-H. Bao, A. Reingruber, P. Dietrich, J. Rui, A. Dück, T. Strassel, L. Li, N.-L. Liu, B. Zhao, and J.-W. Pan, *Nat. Phys.* **8**, 517 (2012).
- [24] R. Zhao, Y. O. Dudin, S. D. Jenkins, C. J. Campbell, D. N. Matsukevich, T. A. B. Kennedy, and A. Kuzmich, *Nat. Phys.* **5**, 100 (2008).
- [25] A. G. Radnaev, Y. O. Dudin, R. Zhao, H. H. Jen, S. D. Jenkins, A. Kuzmich, and T. A. B. Kennedy, *Nat. Phys.* **6**, 894 (2010).
- [26] S.-J. Yang, X.-J. Wang, X.-H. Bao, and J.-W. Pan, *Nat. Photon.* **10**,

381 (2016).

[27] E. Bimbard, R. Boddeda, N. Vitrant, A. Grankin, V. Parigi, J. Stanojevic, A. Ourjoumtsev, and P. Grangier, *Phys. Rev. Lett.* **112**, 033601 (2014).

[28] H. Li, J.-P. Dou, X.-L. Pang, T.-H. Yang, C.-N. Zhang, Y. Chen, J.-M. Li, I. A. Walmsley, and X.-M. Jin, *Optica* **8**, 925 (2021).

[29] K. B. Dideriksen, R. Schmiege, M. Zugenmaier, and E. S. Polzik, *Nat. Commun.* **12**, 3699 (2021).

[30] C. Laplane, P. Jobez, J. Etesse, N. Gisin, and M. Afzelius, *Phys. Rev. Lett.* **118**, 210501 (2017).

[31] K. Kutluer, M. Mazzera, and H. de Riedmatten, *Phys. Rev. Lett.* **118**, 210502 (2017).

[32] S. J. Yang, X. J. Wang, J. Li, J. Rui, X. H. Bao, and J. W. Pan, *Phys. Rev. Lett.* **114**, 210501 (2015).

[33] Y. Yu, F. Ma, X. Y. Luo, B. Jing, P. F. Sun, R. Z. Fang, C. W. Yang, H. Liu, M. Y. Zheng, X. P. Xie, W. J. Zhang, L. X. You, Z. Wang, T. Y. Chen, Q. Zhang, X. H. Bao, and J. W. Pan, *Nature* **578**, 240 (2020).

[34] Y. O. Dudin, A. G. Radnaev, R. Zhao, J. Z. Blumoff, T. A. Kennedy, and A. Kuzmich, *Phys. Rev. Lett.* **105**, 260502 (2010).

[35] X. J. Wang, S. J. Yang, P. F. Sun, B. Jing, J. Li, M. T. Zhou, X. H. Bao, and J. W. Pan, *Phys. Rev. Lett.* **126**, 090501 (2021).

[36] S.-Z. Wang, M.-J. Wang, Y.-F. Wen, Z.-X. Xu, T.-F. Ma, S.-J. Li, and

H. Wang, Communications Physics **4**, 168 (2021).

[37] R. Ikuta, T. Kobayashi, T. Kawakami, S. Miki, M. Yabuno, T. Yamashita, H. Terai, M. Koashi, T. Mukai, T. Yamamoto, and N. Imoto, Nat. Commun. **9**, 1997 (2018).

[38] Y. F. Pu, N. Jiang, W. Chang, H. X. Yang, C. Li, and L. M. Duan, Nat. Commun. **8**, 15359 (2017).

[39] Y. F. Pu, S. Zhang, Y.K. Wu, N. Jiang, W. Chang, C. Li, and L.M. Duan, Nat. Photon. **15**, 374 (2021).

[40] H. Tanji, S. Ghosh, J. Simon, B. Bloom, and V. Vuletic, Phys. Rev. Lett. **103**, 043601 (2009).

[41] C. Liu, Z. Dutton, C. H. Behroozi and L. V. Hau, Nature **409** 490 (2001).

[42] D. Phillips, A. Fleischhauer, A. Mair, R. Walsworth and M. D. Lukin, Phys. Rev. Lett. **86** 783 (2001).

[43] M. D. Eisaman, A. Andre, F. Massou, M. Fleischhauer, A. S. Zibrov, and M. D. Lukin, Nature **438**, 837 (2005).

[44] T. Chaneliere, D. N. Matsukevich, S. D. Jenkins, S. Y. Lan, T. A. Kennedy, and A. Kuzmich, Nature **438**, 833 (2005).

[45] Z. Xu, Y. Wu, L. Tian, L. Chen, Z. Zhang, Z. Yan, S. Li, H. Wang, C. Xie, and K. Peng, Phys. Rev. Lett. **111**, 240503 (2013).

[46] S-Y Zhou, S-C Zhang, C. Liu, J. F. Chen, Jianming Wen, M. M. T. Loy, G. K. L. Wong, and S.-W. Du, Optics express **20**, 24124 (2012).

[47] G. Heinze, C. Hubrich, and T. Halfmann, Phys. Rev. Lett. **111**, 033601 (2013).

[48] Y. H. Chen, M. J. Lee, I. C. Wang, S. Du, Y. F. Chen, Y. C. Chen, and I. A. Yu, Phys. Rev. Lett. **110**, 083601 (2013).

[49] Y. F. Hsiao, P. J. Tsai, H. S. Chen, S. X. Lin, C. C. Hung, C. H. Lee, Y. H. Chen, Y. F. Chen, I. A. Yu, and Y. C. Chen, Phys. Rev. Lett. **120**, 183602 (2018).

[50] P. Vernaz-Gris, K. Huang, M. Cao, A. S. Sheremet, and J. Laurat, Nat. Commun. **9**, 363 (2018).

[51] Z. Yan, L. Wu, X. Jia, Y. Liu, R. Deng, S. Li, H. Wang, C. Xie, and K. Peng, Nat. Commun. **8**, 718 (2017).

[52] E. Saglamyurek, N. Sinclair, J. Jin, J. A. Slater, D. Oblak, F. Bussieres, M. George, R. Ricken, W. Sohler, and W. Tittel, Nature **469**, 512 (2011).

[53] C. Clausen, I. Usmani, F. Bussieres, N. Sangouard, M. Afzelius, H. de Riedmatten, and N. Gisin, Nature **469**, 508 (2011).

[54] E. Saglamyurek, J. Jin, V. B. Verma, M. D. Shaw, F. Marsili, S. W. Nam, D. Oblak, and W. Tittel, Nat. Photon. **9**, 83 (2015).

[55] K. R. Ferguson, S. E. Beavan, J. J. Longdell, and M. J. Sellars, Phys. Rev. Lett. **117**, 020501 (2016).

[56] Y. W. Cho, G. T. Campbell, J. L. Everett, J. Bernu, D. B. Higginbottom, M. T. Cao, J. Geng, N. P. Robins, P. K. Lam, and B. C.

Buchler, Optica **3**, 100 (2016).

[57] M. Sabooni, Q. Li, S. Kroll, and L. Rippe, Phys. Rev. Lett. **110**, 133604 (2013).

[58] N. Sinclair *et al.*, Phys. Rev. Lett. **113**, 053603 (2014).

[59] M. Hosseini, G. Campbell, B. M. Sparkes, P. K. Lam, and B. C. Buchler, Nat. Phys. **7**, 794 (2011).

[60] K. F. Reim, J. Nunn, V. O. Lorenz, B. J. Sussman, K. C. Lee, N. K. Langford, D. Jaksch, and I. A. Walmsley, Nat. Photon. **4**, 218 (2010).

[61] J. Guo, X. Feng, P. Yang, Z. Yu, L. Q. Chen, C. H. Yuan, and W. Zhang, Nat. Commun. **10**, 148 (2019).

[62] D.-S. Ding, W. Zhang, Z.-Y. Zhou, S. Shi, B.-S. Shi, and G.-C. Guo, Nat. Photon. **9**, 332 (2015).

[63] K. T. Kaczmarek, P. M. Ledingham, B. Brecht, S. E. Thomas, G. S. Thekkadath, O. Lazo-Arjona, J. H. D. Munns, E. Poem, A. Feizpour, D. J. Saunders, J. Nunn, and I. A. Walmsley, Phys. Rev. A **97**, 042316 (2018).

[64] Ran Finkelstein, Eilon Poem, Ohad Michel, Ohr Lahad, and O. Firstenberg, Sci. Adv. **4**, eaap8598 (2018).

[65] C. Simon, H. de Riedmatten, M. Afzelius, N. Sangouard, H. Zbinden, and N. Gisin, Phys. Rev. Lett. **98**, 190503 (2007).

[66] K. C. Cox, D. H. Meyer, Z. A. Castillo, F. K. Fatemi, and P. D. Kunz, Phys. Rev. Lett. **123**, 263601 (2019).

[67] L. Heller, P. Farrera, G. Heinze, and H. de Riedmatten, Phys. Rev.

[68] See Supplemental Material

## Figures and Figure Captions

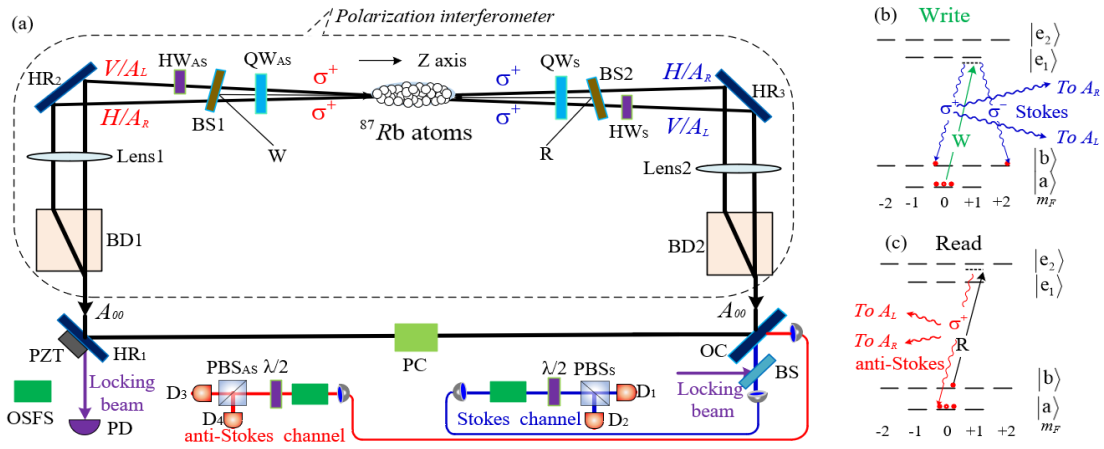


**Fig. 1.** Schematic diagram for experimental setup (a): A polarization interferometer formed by two beam displacers (BD1 and BD2) is inserted into a ring cavity. A locking laser pulse is coupled to the  $A_{00}$  mode through a beam splitter (BS). Leaks of the cavity-locking pulse from  $HR_3$  are detected by a fast photodiode (PD) to generate error signals. The error signals are amplified and used to drive a piezoelectric transducer (PZT) to stabilize the cavity length. OSFS: optical-spectrum-filter set [36]; PC: phase compensator; BS1 (BS2): non-polarizing beam splitter with a reflectance of 1% (3%). (b) and (c) are relevant atomic levels involved in the write and read processes, respectively, W (R): write (read) laser.

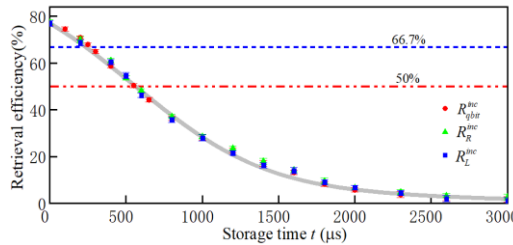


**Fig. 2** Intrinsic retrieval efficiencies as a function of storage time  $t$  for  $\chi=1\%$ . Error bars represents 1 standard deviation.

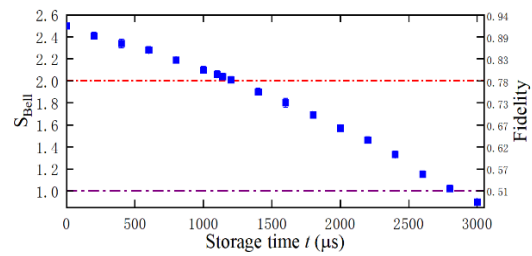


**Fig. 3.** Measured Bell parameter as a function of storage time  $t$  for  $\chi=2\%$ . Error bars represent 1 standard deviation.

**Supplementary material to “Generation of highly-retrievable atom–  
photon entanglement with a millisecond lifetime via a  
spatially-multiplexed cavity”**

Minjie Wang, Shengzhi Wang, Tengfei Ma, Ya Li, Yan Xie, Haole Jiao,  
Hailong Liu, Shujing Li, Hai Wang<sup>\*</sup>

The State Key Laboratory of Quantum Optics and Quantum Optics  
Devices,

Institute of Opto-Electronics, Shanxi University, Taiyuan 030006

China Collaborative Innovation Center of Extreme Optics,  
Shanxi University, Taiyuan 030006, China

**Two-mode ring cavity based on polarization interferometer**

As shown in the Fig.1 in the main text, our experimental setup is mainly formed by the ring optical cavity inserted by the polarization interferometer with cold atoms in it. As mentioned in the main text, the ring cavity is formed by three flat mirrors ( $HR_{1,2,3}$ ) and a flat output coupler (OC). The cold atoms are placed at location  $O$ . To explain our experimental scheme, we firstly discuss the ring cavity without the polarization interferometer, which is shown in Fig.S1.

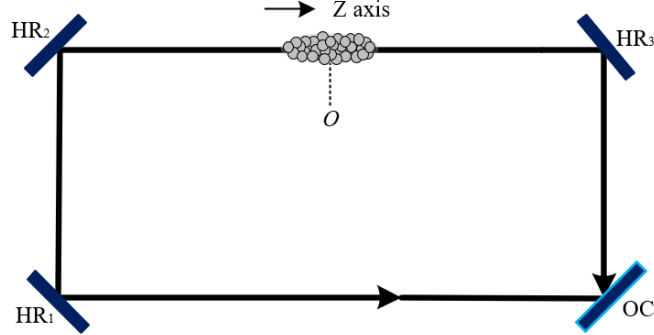


**Fig.S1** Ring cavity without the polarization interferometer

The transfer (ABCD) matrix of the ring cavity with a length of  $L$  is given by  $T_{c1} = \begin{bmatrix} A & B \\ C & D \end{bmatrix} = \begin{bmatrix} 1 & L \\ 0 & 1 \end{bmatrix}$ , which show that the ring cavity satisfy the critical condition  $(A+D)/2=1$ . By aligning the cavity mirrors, we may make a TEM<sub>00</sub> light beam, which has a small divergence angle, bounce back and forth in the cavity. The propagating path of the cavity mode  $A_{00}$  denotes as the black line in Fig.S1. To decrease the escaping loss of the mode  $A_{00}$  when it propagates in the cavity, we set its spot size (diameter) to be large, whose value is 5.2 mm in our presented experiment. The measured loss of the mode  $A_{00}$  escaping from the cavity per round trip is  $\sim 2.7\%$ , which is far less than the 20% transmission of OC and allows the mode  $A_{00}$  to serve as the cavity mode. As shown in Fig. S1, the  $A_{00}$  cavity mode goes through the cold atoms, which is coincided with the  $z$ -axis during the path from  $HR_2$  to  $HR_3$ . In our experiment, the  $z$ -axis is quantum direction defined by a bias magnetic field (4G), along which the write beam is applied.

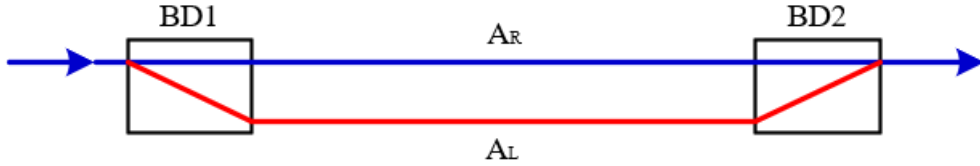


**Fig.S2** A common polarization interferometer

A common polarization interferometer is formed by two identical beam displacers (BD1 and BD2) separated by a distance. Fig.S2 shows the configuration of the common polarization interferometer, where, an arbitrarily-polarized light beam moves towards the right and enters the BD1. The BD1 split the light beam into *H*-polarized and *V*-polarized components. Both beam components direct into  $A_R$  and  $A_L$  arms of the interferometer, respectively, parallel propagate, and then are recombined into a light beam by BD2.

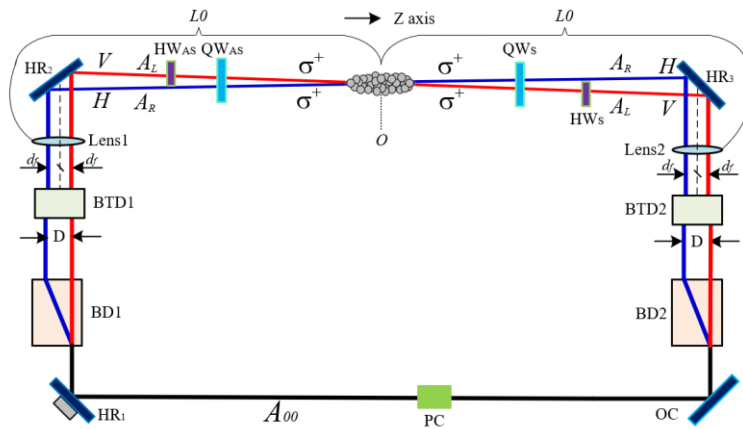


**Fig.3S** Diagram of the two-mode ring cavity based on the polarization interferometer

In our experimental set-up, the polarization interferometer is combined into the ring cavity and the two arms are required to couple with the cold atomic ensemble. For which, BD1 (BD2) is inserted in between HR<sub>1</sub> and

HR<sub>2</sub> (HR<sub>3</sub> and OC) and two lenses (lens1 and lens2) are inserted in between two beam displacers. As shown in Fig.S3, the lens1 (lens2) is inserted in between BD1 and HR<sub>2</sub> (between BD2 and HR<sub>3</sub>). For setting the polarizations of the two arms to be a specific polarization ( $\sigma^+$ -polarization), we insert the  $\lambda/4$  wave-plates QW<sub>AS</sub> and QW<sub>S</sub> in the two arms and  $\lambda/2$  wave-plates QW<sub>AS</sub> and QW<sub>S</sub> only in  $A_L$  arm. The optical axis of BD1 (BD2) is arranged to be parallel with the  $A_{00}$  path line in the cavity. The lengths from the lens1 or lens2 to the atomic center  $O$  is  $L_0$ . Both lenses have the same focal length  $F_0 = L_0$ . We also insert two beam-transformation devices, i.e., BTD1 and BTD2, in between BD1 and lens1 and BD2 and lens2, respectively. BTD1 (BTD2) is formed by two lenses, which can shrink (expand) the two-separation distance between the two arms by a factor of  $F_{BTD}$  when they propagate along clockwise [1]. Importantly, the two arms remain parallel after going through BTD. We now explain the paths of the two arms of the interferometer and then discuss the reason for introducing the BTDs. When  $A_{00}$  mode propagates along clockwise in the cavity, it will be split into  $H$ - and  $V$ - polarized components by BD1. The  $H$ -polarized and  $V$ -polarized components of the  $A_{00}$  mode propagate in the two arms ( $A_R$  and  $A_L$ ), respectively, whose separation distance denotes by  $D$ . After going through BTD1, the arms  $A_R$  and  $A_L$  still propagate parallel but their distance reduces to  $D/F_{BTD}$ . As shown in Fig.S3, we carefully arrange the lens1 to make the distance

from its main optical axis (dashed line) to the  $A_R$  or  $A_L$  path line be all equal to  $d_f$ . Both components of the  $A_{00}$  mode are reflected by  $\text{HR}_2$ . The  $V$ -polarized component is transformed into  $H$ -polarization by the  $\lambda/2$ -wave-plate  $\text{HW}_{\text{AS}}$ . Subsequently, both  $H$ -polarized components are transformed into  $\sigma^+$ -polarization by the  $\lambda/4$ -wave-plate  $\text{QW}_{\text{AS}}$  and then crossways go through the atoms (the location  $O$ ). The angle between the arm  $A_R$  ( $A_L$ ) and the write beam (along z-axis) is given by  $\theta_R = d_f / L_0$  ( $\theta_L = d_f / L_0$ ). Next, both  $\sigma^+$ -polarized components are transformed into  $H$ -polarization by the  $\lambda/4$ -wave-plate  $\text{QW}_S$ . The  $H$ -polarized component in  $A_L$  arm is transformed into  $V$ -polarization by the  $\lambda/2$ -wave-plate  $\text{HW}_S$ . After reflected by  $\text{HR}_3$ , both components go through the lens2. We also arrange the lens2 to make the distances from its main optical axis to the  $A_R$  or  $A_L$  arm be all equal to  $d_f$ . After the lens2, the two arms parallel propagate, whose separation distance is  $D/F_{BTD}$ , which is the same as that before the lens1. The two arms go through  $\text{BTD}2$ , which expand their separation distance by the factor of  $F_{BTD}$ . Thus, after  $\text{BTD}2$ , the separation distance of the two arms is transformed back into  $D$ . The two arms parallel propagate and enter the  $\text{BD}2$ , which combine the two arms into the  $A_{00}$  mode. In our presented experiment, the distance between lens1 and lens2 is carefully set to be  $2F_0$  in order to enable the combination of the two arms via  $\text{BD}2$  is perfect. The measured loss of the mode  $A_{00}$  via  $A_R$  ( $A_L$ ) path escaping from cavity per round trip is  $\sim 3.2\%$

(3.2%), showing that the interferometer-based cavity supports the  $A_R$  and  $A_L$  arms to serve as cavity modes.

In our experiment, we have to individually operate polarizations of the Stokes (anti-Stokes) photons propagating in the arms  $A_R$  and  $A_L$ . For example, we insert the  $\lambda/2$  wave-plate  $HW_{AS}$  ( $HW_S$ ) only in the  $A_L$  arm after BD1(BD2), which transform its  $H$ -polarization to  $V$ -polarization. For achieving the individual polarization operations, the separation distance  $D$  between the two arms is required to be more than the diameter of the cavity mode  $A_{00}$ . In our presented experiment, we set  $D=5.5$  mm, which is larger than the diameter of  $A_{00}$ . Without the BTDs, the separation distance of the two arms at lens1 (lens2) will be  $D=2d_f=5.5$  mm. To achieve a long-lived memory, we have to suppress decoherence due to atomic motions, which in turn require to achieve long wave-length SW storage and then decrease the angle  $\theta_R$  ( $\theta_L$ ) [1]. With BTD1, the separation distance  $2d_f$  at the lens1 (lens2) is changed into  $2d_f=D/F_{BTD}$ . To achieve small values of the angles, we use the lenses with  $F_0=1.5$  m and BTD1 with factor of  $F_{BTD}=2$ . So, the angles can be given as  $\theta_R=\theta_L=d_f/(F_{BTD}L_0)=d_f/(F_{BTD}F_0)\approx 0.053^0$ , which corresponds to a millisecond lifetime [1]. It is noted that for briefly and clearly explaining the ring cavity combined with the polarization interferometer, we neglected the BTDs in the Fig.1 in the main text.

In our presented experiment, the measured total cavity loss is  $\sim 13\%$ ,

which includes: (1) Transmission losses due to the non-polarization beam splitters BS1 and BS2 (see Fig.1 in the main text), which are 1% and 3%, respectively; (2) Optical loss due to imperfect reflections of  $HR_{1,2,3}$ , which is 1%; (3) Transmission losses of the optical elements (BDs, BTDs, lens1,2, and wave-plates, *et.al.*), which is 4.8%; (4) Loss of the mode  $A_R$  ( $A_L$ ) escaping from the cavity per round trip, which is 3.2% (3.2%). The length of the ring cavity is  $\sim 6$  m, corresponding to a free spectral range of 50 MHz. The refection rate of the OC is  $\sim 80\%$ . The cavity has finesse of 16.9 and 17.0 for the modes  $A_R$  and  $A_L$ . The spot sizes of both modes at the location  $O$  (the center of the atoms) are all  $\sim 0.5$ mm.

The dispersion of the Stokes and anti-Stokes fields due to the beam displacers is very small and then can be neglected. In our experiment, the relative phase between two Stokes (anti-Stokes) fields propagating from BD1 to BD2 via  $A_R$  and  $A_L$  arms is compensated to be zero with the phase compensator (labeled as PC in Fig.1). Thus, the sum of  $\varphi_s$  and  $\varphi_{AS}$  is set to zero. Since the phase compensator is formed by wave-plates [1], this phase compensation is passively. By changing the frequency of the write (read) laser beam, we tune the frequency of the Stokes (anti-Stokes) field and then make Stokes (anti-Stokes) field resonate with the cavity. The Stokes emissions into  $A_R$  and  $A_L$  modes are both enhanced by a factor of  $2F/\pi$  by the cavity. Also, the efficiencies for retrieving the two SWs  $M_R$  and  $M_L$  are enhanced through the Purcell effect [2].

## Experimental details

The experiment is performed in a cyclic fashion. In each experimental cycle, the durations for preparing cold atoms and running the experiment for spin-wave-photon entanglement (SWPE) generation are 42 ms and 8 ms, respectively, corresponding to a 20-Hz cycle frequency. During the preparation stage, more than  $10^8$  atoms of  $^{87}\text{Rb}$  are trapped in a two-dimensional magneto-optical trap (MOT) for 41.5 ms and further cooled via Sisyphus cooling for 0.5 ms. The cloud of cold atoms has a size of  $\sim 5 \times 2 \times 2 \text{ mm}^3$ , a temperature of  $\sim 100 \text{ }\mu\text{K}$ , and an optical density of  $\sim 16$ . At the end of this preparation stage, a bias magnetic field of  $B_0=4 \text{ G}$  is applied along the  $z$ -axis (see Fig. 1a), and the atoms are optically pumped into the initial level  $|5^2S_{1/2}, F=1, m=0\rangle$ . After the preparation stage, the 8-ms experimental run containing a large number of SWPE-generation trials starts. At the beginning of a trial, a write pulse with a duration of  $\sim 300 \text{ ns}$  is applied to the atomic ensemble to generate correlated pairs of Stokes photons and spin-wave excitations. The detection events at the Stokes detectors  $D_1$  and  $D_2$  in Fig. 1a are analyzed with a field-programmable gate array (FPGA). As soon as a Stokes photon qubit is detected by either one of these detectors, SWPE is generated and the FPGA sends out a feed-forward signal to stop the write processes. After a storage time  $t$ , a read laser pulse with a duration of  $\sim 300 \text{ ns}$  is applied to the atoms to convert the spin-wave qubit into the

anti-Stokes photon qubit. After a 1300-ns interval, a cleaning pulse with a duration of 200 ns is applied to pump the atoms into the initial level  $|5^2 S_{1/2}, F=1, m=0\rangle$ . Then, the next SWPE-generation trial starts. However, in most cases, the Stokes photon is not detected during the write pulse owing to the low excitation probability ( $\chi \leq 2\%$ ). If this is the case, the atoms are pumped directly back into the initial level by the read and cleaning pulses. Subsequently, the next trial starts, i.e., the write pulse is applied. The delay between the two adjacent write pulses for a storage time of  $t \approx 1 \mu\text{s}$  is 2000 ns. Therefore, the 8-ms experimental run contains  $\sim 4000$  experimental trials. Considering that a 1-s experiment contains 20 cycles, the repetition rate of the SWPE-generation trail is  $r = 8 \times 10^4$ .

The powers of the two beams applied onto the atoms are  $\sim 300 \mu\text{W}$  and  $\sim 10 \text{ mW}$ , respectively. The read laser is red-detuned by 110 MHz to the transition  $|b\rangle \rightarrow |e_2\rangle$ . To block the write (read) laser beam in the Stokes and anti-Stokes channels, we place an optical-spectrum-filter set (OSFS) before each polarization beam splitter PBS<sub>S</sub> (PBS<sub>AS</sub>). Each OSFS comprises five Fabry–Perot etalons, which attenuate the write (read) beam by a factor of  $\sim 8.1 \times 10^{-12}$  ( $\sim 3.8 \times 10^{-11}$ ) and transmit the Stokes (anti-Stokes) fields with a transmission of  $\sim 56\%$ . Additionally, in the Stokes (anti-Stokes) detection channel, the spatial separation of the Stokes (anti-Stokes fields) from the strong write (read) beam attenuates the write (read) beam by a factor of  $\sim 10^{-4}$ . In this experiment, we

measured the uncorrelated noise probability in the anti-Stokes mode, which is  $p_N \approx 10^{-4}$  per read pulse (300 ns). Such uncorrelated noise mainly results from the leakage of the read beam into the anti-Stokes detection channel.

The efficiency of the Stokes (anti-Stokes) photons escaping from the ring cavity is defined as  $\eta_{esp} = \frac{T_{OC}}{T_{OC} + L}$ , where  $T_{OC} = 20\%$  is the transmission of the output coupler mirror, and  $L \approx 13\%$  is the cavity total loss. Thus, we have  $\eta_{esp} \approx 60.6\%$ .

The transmission efficiency  $\eta_T$  of the Stokes (anti-Stokes) photons from the cavity to the detectors includes the coupling efficiency  $\eta_{SMF} \approx 0.71$  of the single-mode fiber SMF<sub>AS</sub>, the transmission  $\eta_{Filter} \approx 0.56$  of the optical-spectrum-filter set (OSFS), and the transmission  $\eta_{MMF} \approx 0.92$  of the multi-mode fiber. Therefore,  $\eta_T = 0.71 \times 0.56 \times 0.92 \approx 36.6\%$ .

The total efficiency of detecting the Stokes (anti-Stokes) photon is given by  $\eta_{TD} = \eta_{esp} \times \eta_T \times \eta_D$ , where  $\eta_D$  is the quantum efficiency of the single-photon detectors ( $D_1$ ,  $D_2$ ,  $D_3$  and  $D_4$ ), whose value is  $\eta_D \approx 68\%$  in our experiment. So, we have  $\eta_{TD} = \eta_{esp} \times \eta_T \times \eta_D \approx 15\%$ .

All error bars in the experimental data represent a  $\pm 1$  standard deviation, which is estimated from Poissonian detection statistics using Monte Carlo simulations.

For comparison, we plot Fig. S4 in Supplementary material [68] to show the measured retrieval efficiencies for the qubit storages as functions of

storage times in previous works [3-9]. Our result of storage time of 540  $\mu$ s (230  $\mu$ s) at 50% (66.7%) intrinsic retrieval efficiency is 13.5 (24) times longer than the previously reported best result [3] ([4]).

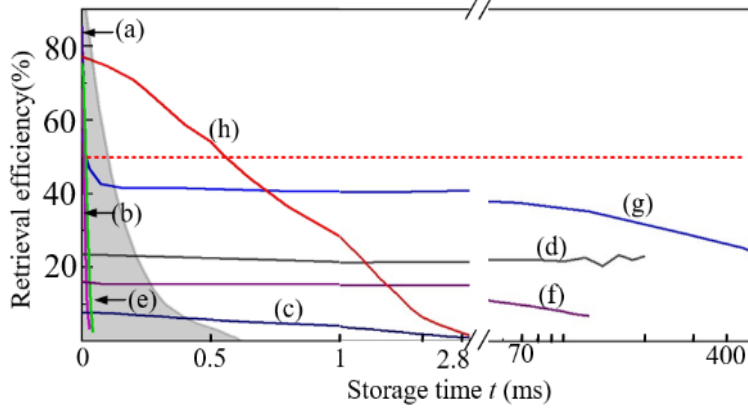


**Fig. S4.** Retrieval efficiencies of memory qubit vs storage time  $t$  in various systems. The shaded region shows the result for an ideal-optical-fiber loop. Curves (a) and (b) are the results for storages of single-photon [5] and weak-coherent-light [6] qubits via EIT in high-optical-density cold atoms. Curve (c) represents the results for qubit memory stored as MFI spin waves via EIT in cold atoms [7]. Curve (d) represents single-photon qubit storage via EIT in single atoms [8]. Curves (e), (f), (g) and (h), corresponding to the results in Refs. [3], [9], [4] and our experiment, respectively, represent qubit memories via DLCZ protocol.

### Improvement on the total detection efficiencies

The low total detection efficiency can be effectively improved in future work. Assuming that the cavity loss reduces to 1%, the cavity escaping efficiency  $\eta_{esp}$  will be up to  $\sim 95\%$ . Furthermore, the efficiencies  $\eta_{SMF_s}$ ,  $\eta_{Filter}$ , and  $\eta_{MMF}$  can be greatly improve to  $\sim 99\%$ ,  $\sim 99\%$ , and  $\sim 99\%$ . One can also use superconductor single-photon detectors with a detection efficiency of 95% [9] instead of silicon-avalanche-photodiode single-photon detectors. With the aforementioned improvements, the total

detection efficiency would change to

$$\eta_{TD} = \eta_{esp} \times \eta_{SMF_S} \times \eta_{Filter} \times \eta_{MMF} \times \eta_D \approx 0.98 * 0.99 * 0.98 * 0.99 * 0.95 \approx 88\% .$$

**Repeater rates for distributing an entangled photon pair over distances up to 1000 km through a multiplexed QR using cavity-perfectly-enhanced or cavity-imperfectly-enhanced schemes**

On the basis of two-photon interference, the repeater rate for distributing an entangled photon pair over a distance  $L$  through multiplexed [10-13] DLCZ QR protocols with nest level  $n$  can be evaluated by the following equation [8]:

$$R_{rate} \approx \frac{1}{T_{cc}} P_0^{(N)} \left( \prod_{j=1}^{j=4} P_j \right) P_{pr} , \quad (S1)$$

where  $T_{cc} = L_0 / c$  is the communication time with  $c$  being the speed of light in fibers and  $L_0 = L / n$  the distance between two nodes belonging to an elementary link;  $P_0^{(N)} = 1 - (1 - P_0)^N \approx NP_0$  is the success probability for entanglement generation in an individual elementary link using multiplexed nodes that each store  $N$  qubits, with  $P_0 = (\chi^2 e^{-L_0 / L_{att}} \eta_{FC}^2 \eta_{TD}^2) / 2$  being that using non-multiplexed nodes,  $\eta_{FC}$  being the memory-to-telecom frequency conversion efficiency,  $\eta_{TD}$  being the total detection efficiency, and the factor 1/2 being due to double-excitation events from a single node [14,15];  $P_j = \left[ \left( R_0 e^{-t_{j-1} / \tau_0} \right)^2 \eta_{TD}^2 \right] / 2$  with  $j = 1$  to  $n = 4$  is the success probability for entanglement swapping at the

$i$ -th level, with  $\tau_0$  the lifetime of the multiplexed node memory based on an atomic ensemble, and  $R_0$  the qubit retrieval efficiency of the memory at zero delay;  $t_0 \simeq T_{cc} / P_0^{(N)} = T_{cc} / (NP_0)$  is the time needed for the elementary entanglement generation;  $t_j \simeq t_{j-1} / P_j$   $j = 1$  to  $n = 4$  is the time needed for the  $i$ th-level entanglement swapping; and  $P_{pr} \approx (R_0 e^{-t_4/\tau_0})^2 / 2$  is the probability for distributing an entangled photon pair over the distance  $L$ .

In an optical EIT storage [16], the  $1/e$  lifetime of  $\tau_0 = 16$  s by applying dynamic decoupling pulse sequences has been achieved. Quantum memories with comparable storage time may be within reach. The multiplexed storages of qubits with hundreds of spatial modes [17] and tens of temporal modes [18] have been demonstrated via DLCZ protocol in cold atoms. Thus, one can achieve multiplexed qubit memories with thousands of modes by combining both schemes [19, 20] into individual systems. For the case that high-performance quantum technologies including large-scale-multiplexing (e.g., 1000 modes), cavity-enhanced-retrieval and long-lifetime (16 s) quantum storages, high-efficiency memory-to-telecom frequency conversion (with efficiency of 33%) [15] as well as superconductor single-photon detections [9] (with efficiency of 95%) are integrated into individual repeater nodes, we calculate the repeater rate for distributing an entangled photon pair over distance  $L$  through 4-level QR through Eq.(S1) and

present the results in Fig.S1. The blue solid and red dashed curves are the results for the cases of using cavity-perfectly-enhanced (CPE) retrieval ( $R_0 \approx 80\%$ ) and cavity-imperfectly-enhanced (CIE) retrieval ( $R_0 \approx 60\%$ ) schemes, respectively, where, the other parameters are the same. For a fixed repeater rate of  $10^{-4}$ , one can see that the QR using CPE-retrieval nodes may achieve an entangled photon pair distribution over  $L \approx 1000\text{km}$  km, while that using CIE retrieval nodes may only achieve entanglement distribution over  $L \approx 430\text{km}$  km, showing a significant advance of CPE over CIE retrieval schemes.

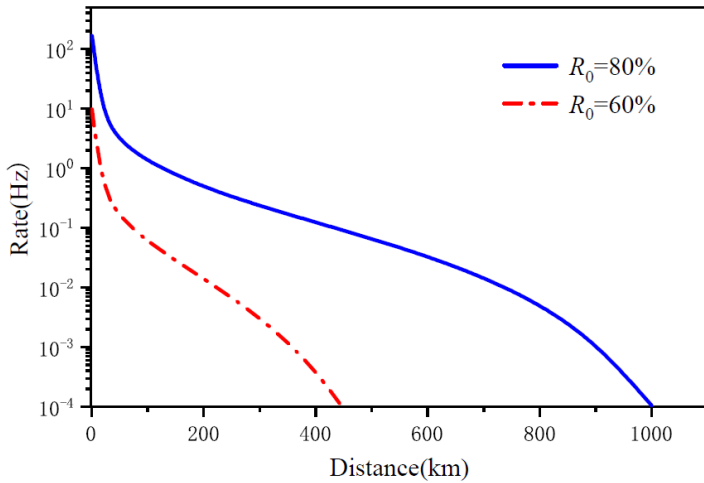


**Fig.S5** Calculated repeater rates as functions of entanglement distribution over distance  $L$  according to Eq. S1, where the blue solid (red dash) curve corresponds to the quantum repeater using nodes with zero-delay retrieval efficiency  $R_0 \approx 80\%$  ( $R_0 \approx 60\%$ ). The parameters used in the calculation are: nest level  $n=4$ , mode number  $N=1000$ , memory lifetime  $\tau_0 = 16\text{ s}$ , total detection efficiency  $\eta_{TD} \approx 88\%$  for the Stokes (anti-Stokes) detection channel, and quantum frequency conversion efficiency  $\eta_{FC} = 33\%$ .

## Reference

- [1] S.-Z. Wang, M.-J. Wang, Y.-F. Wen, Z.-X. Xu, T.-F. Ma, S.-J. Li, and H. Wang, *Communications Physics* **4**, 168 (2021).
- [2] X.-H. Bao, A. Reingruber, P. Dietrich, J. Rui, A. Dück, T. Strassel, L. Li, N.-L. Liu, B. Zhao, and J.-W. Pan, *Nat. Phys.* **8**, 517 (2012).
- [3] S. J. Yang, X. J. Wang, J. Li, J. Rui, X. H. Bao, and J. W. Pan, *Phys. Rev. Lett.* **114**, 210501 (2015).
- [4] X. J. Wang, S. J. Yang, P. F. Sun, B. Jing, J. Li, M. T. Zhou, X. H. Bao, and J. W. Pan, *Phys. Rev. Lett.* **126**, 090501 (2021).
- [5] Y. Wang, J. Li, S. Zhang, K. Su, Y. Zhou, K. Liao, S. Du, H. Yan, and S.-L. Zhu, *Nat. Photon.* **13**, 346 (2019).
- [6] P. Vernaz-Gris, K. Huang, M. Cao, A. S. Sheremet, and J. Laurat, *Nat. Commun.* **9**, 363 (2018).
- [7] Z. Xu, Y. Wu, L. Tian, L. Chen, Z. Zhang, Z. Yan, S. Li, H. Wang, C. Xie, and K. Peng, *Phys. Rev. Lett.* **111**, 240503 (2013).
- [8] Y. O. Dudin, A. G. Radnaev, R. Zhao, J. Z. Blumoff, T. A. Kennedy, and A. Kuzmich, *Phys. Rev. Lett.* **105**, 260502 (2010).
- [9] E. L. Adriana, J. M. Aaron, W. N. Sae, *Opt. Express* **16**, 3032 (2008).
- [10] C. Simon, H. de Riedmatten, M. Afzelius, N. Sangouard, H. Zbinden, and N. Gisin, *Phys. Rev. Lett.* **98**, 190503 (2007).
- [11] O. A. Collins, S. D. Jenkins, A. Kuzmich, and T. A. Kennedy, *Phys.*

Rev. Lett. **98**, 060502 (2007).

[12] D. Lago-Rivera, S. Grandi, J. V. Rakonjac, A. Seri, and H. de Riedmatten, Nature **594**, 37 (2021).

[13] X. Liu, J. Hu, Z. F. Li, X. Li, P. Y. Li, P. J. Liang, Z. Q. Zhou, C. F. Li, and G. C. Guo, Nature **594**, 41 (2021).

[14] B. Zhao, Z. B. Chen, Y. A. Chen, J. Schmiedmayer, and J. W. Pan, Phys. Rev. Lett. **98**, 240502 (2007).

[15] Y. Yu, F. Ma, X. Y. Luo, B. Jing, P. F. Sun, R. Z. Fang, C. W. Yang, H. Liu, M. Y. Zheng, X. P. Xie, W. J. Zhang, L. X. You, Z. Wang, T. Y. Chen, Q. Zhang, X. H. Bao, and J. W. Pan, Nature **578**, 240 (2020).

[16] Y. O. Dudin, L. Li, and A. Kuzmich, Phys. Rev. A **87**, 031801(R) (2013).

[17] M. Lipka, M. Mazelanik, A. Leszczyński, W. Wasilewski, and M. Parniak, Communications Physics **4**, 46 (2021).

[18] Y. Wen, P. Zhou, Z. Xu, L. Yuan, H. Zhang, S. Wang, L. Tian, S. Li, and H. Wang, Phys. Rev. A **100**, 012342 (2019).

[19] N. Sinclair, E. Saglamyurek, H. Mallahzadeh, J. A. Slater, M. George, R. Ricken, M. P. Hedges, D. Oblak, C. Simon, W. Sohler, and W. Tittel, Phys. Rev. Lett. **113**, 053603 (2014).

[20] Tian-Shu Yang, Zong-Quan Zhou, Yi-Lin Hua, Xiao Liu, Zong-Feng Li, Pei-Yun Li, Yu Ma, Chao Liu, Peng-Jun Liang, Xue Li, Yi-Xin Xiao, Jun Hu, Chuan-Feng Li, Guang-Can Guo, Nat. Commun. **9**, 3407 (2018).

